Journal of Experimental Nanoscience
Publication details, including instructions for authors and subscription information:
http://www.informaworld.com/smpp/title~content=t716100757

Reverse micelles used as templates: a new understanding in nanocrystal growth

M. P. Pileni[a]
[a] Laboratoire LM2N, Université P. et M. Curie (Paris VI), F-75231 Paris Cedex 05, France

Online publication date: 28 September 2010

To cite this Article Pileni, M. P.(2006) 'Reverse micelles used as templates: a new understanding in nanocrystal growth', Journal of Experimental Nanoscience, 1: 1, 13 — 27
To link to this Article: DOI: 10.1080/17458080500462075
URL: http://dx.doi.org/10.1080/17458080500462075

Journal of Experimental Nanoscience,
Vol. 1, No. 1, March 2006, 13–27

Taylor & Francis
Taylor & Francis Group

Reverse micelles used as templates: a new understanding in nanocrystal growth

M. P. PILENI*

Laboratoire LM2N, Université P. et M. Curie (Paris VI), BP 52, 4 Place Jussieu, F–75231 Paris Cedex 05, France

(*Received October 2005; in final form November 2005*)

In this paper we demonstrate that reverse micelles make possible the homogeneous growth of nuclei to nanocrystals with similar shapes. Furthermore, hydrazine increases the relative percentage of tetrahedral nuclei with selective adsorption during crystal growth, favouring the formation of nanodisks.

1. Introduction

In the last few years, there has been a very great expansion in research into inorganic nanocrystals because of their high application potentiality [1]. This involves biology, electronics, transport, information technology, and implies producing nanocrystals with well-defined sizes, shapes and crystallinity. In fact, the electrical, optical and magnetic properties of inorganic nanomaterials vary widely with these various factors. Several challenges have to be faced. We must produce large amounts and well-defined materials and be able to manipulate these nanocrystals. Because of the high potentiality of these systems, several approaches [2–16] to produce these nanomaterials have been undertaken in the last decade. Controlling the nanocrystal shape is a real challenge and more data are now needed to ascertain the general principles that determine this shape. This is probably due to the fact that anisotropic materials are not in their thermodynamically stable state. Crystal growth on the nanoscale seems to follow behaviour similar to that of the bulk phase [17]. Most of the changes are based on the existence of a more or less epitaxial adsorption layer on the crystal, which is composed of solvent, salts or impurities. Their precise roles are as yet uncertain but it appears that the latter lead to an increase in the growth rate of certain faces. From these observations, we can ask why templates made of surfactants are quite effective in controlling the formation of nanospheres whereas rather large exceptions are seen for anisotropic shapes. This is probably due to the structure of the colloidal templates with or without free surfactant present in the bulk phase. The energy needed to

*Email: pileni@sri.jussieu.fr

Journal of Experimental Nanoscience
ISSN 1745-8080 print/ISSN 1745-8099 online
http://www.tandf.co.uk/journals
DOI: 10.1080/17458080500462075

produce spherical nanocrystals is less than that for producing anisotropic nanocrystals. A general method for controlling nanocrystal shapes through soft chemistry has not yet been found but this does not mean that such a method will not be discovered.

Here, we demonstrate, for silver and copper nanocrystals, that reverse micelles are good candidates for producing nanocrystals having the same shapes as their nuclei. Furthermore, the amount of hydrazine seems to be the key parameter in the production of face-centred-cubic (fcc) single crystal nanodisks, whereas the influence of the surfactant molecules when they are self-assembled at the oil–water interface remains negligible. The effect of the surfactant in nanocrystal growth has thus been revised. With highly pure surfactant molecules self-organized to form water-in-oil droplets, its influence on nanocrystal growth is negligible. The amount of reducing agent such as hydrazine plays an important role. A surfactant moving freely in the growth medium perturbs the nanocrystal growth.

2. Reverse micellar properties [18]

Reverse micelles are water-in-oil droplets stabilized by a surfactant. The surfactant most often used is sodium 2 bis (2-ethylhexyl)sulfosuccinate, usually called Na(AOT). These droplets are displaced randomly and subjected to Brownian motion. They exchange their water content and re-form two distinct micelles. Furthermore, the size of the water-in-oil droplets increases linearly, i.e. the micellar concentration decreases, with increasing the water content, defined as $w = [H_2O]/[AOT]$. Let us consider two reactants A (such as silver or copper ions) and B (such as hydrazine) solubilized in two distinct micellar solutions. On mixing them, and because of the exchange process, A and B are in contact and react. It is thus possible to induce a very wide range of chemical reactions. At fixed surfactant and reactant concentration, the number of reactants per micelle increases, following a Poisson distribution. On increasing w, the water structure inside the droplet evolves from a morphology similar to ice to free water and consequently the solvation of the counter-ions inside the droplet increases [19]. This induces a change in the chemical reaction yield (i.e. redox potential, solubility, etc.). Above $w = 10$, the counter-ions of the surfactant are hydrated and 'free' bulk water appears in the droplets [20].

Reverse micelles have been used for almost 17 years to produce a very wide range of nanocrystals such as II-VI semiconductors, metals, etc. [5, 21]. With silver and copper nanocrystals, no traces of oxide are detected. This is mainly attributed to the fact that a functionalized surfactant (i.e. the head polar group of the surfactant is one of the reactants) is used to produce nanocrystals [22]. At a fixed reactant concentration, the increase in the water content induces an increase in the number of reactants per micelle and in the amount of solvated reactant ions.

3. Results

We know from crystal growth that the origin of the material structure is related to the constituent nuclei. Bulk silver and copper metal materials have fcc structures and

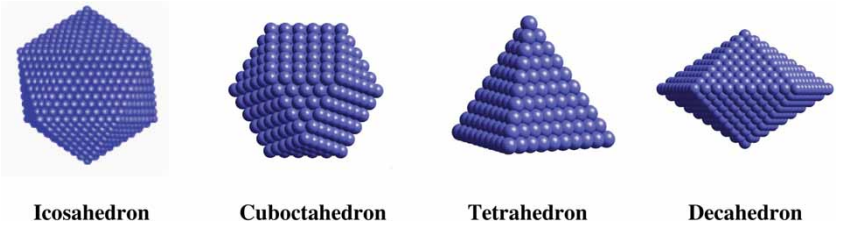

Figure 1. Representation of the stable precursor nuclei for the formation of copper nanocrystals. This figure is available in colour online.

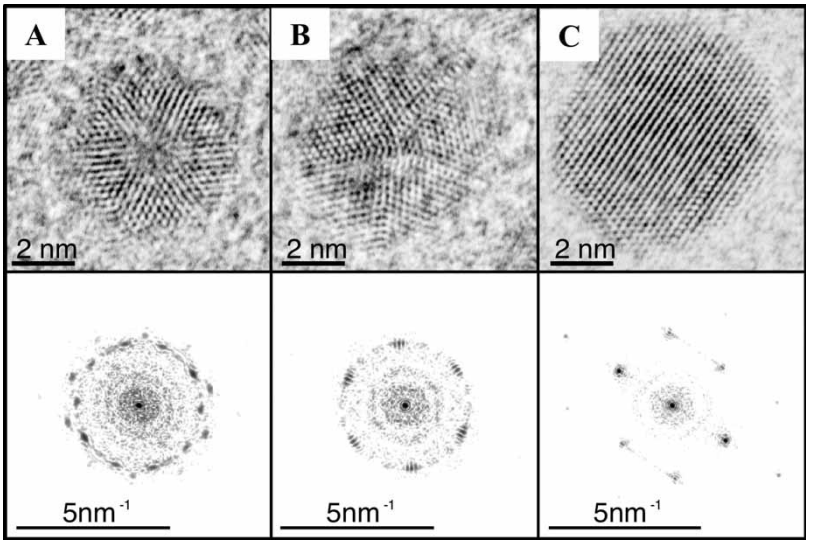

Figure 2. Silver nanocrystals. Top: HRTEM images; bottom: power spectra. (A) Decahedron viewed along the five-fold axis; (B) icosahedron viewed along the three-fold axis; (C) cubooctahedron in the [110] orientation.

their nuclei are icosahedral, decahedral, cubooctahedral and tetrahedral [23] (figure 1). In the following the percentage of nanocrystals differing by their shapes and sizes is determined by counting more than 500 particles. The experiments have been repeated several times and the percentages remain similar.

Silver nanocrystals with 5 nm average diameter are produced from reverse micelles ($R = 2.4$, $w = 2$; see the appendices). At the end of the synthesis the nanoparticles are extracted from the micelles and their crystallinity is studied [24]. The electron diffraction pattern shows a reflectance characteristic of an fcc structure. Spots, corresponding to various orientations of the nanocrystals, appear inside the concentric rings, which clearly shows that the nanoparticles have good crystallinity. The high-resolution transmission electron microscopy (HRTEM) images and power spectra, i.e. the calculated square of the Fourier transform of the image (see below each TEM image in figure 2), give additional information on the nanocrystal structure. Decahedron nanocrystals viewed along the five-fold axis are shown in figure 2(A) and an

icosahedron viewed along the three-fold axis with three pairs of (111) reflections is shown in figure 2(B). These two structures originate from the twinning of 5 and 20 tetrahedral subunits, respectively, and are called multiply twinned particles, MTPs (figure 2B). Figure 2(C) shows the formation of a cubooctahedron with an fcc structure in the [110] orientation. From this structural investigation, Ag nanoparticles appear to be highly crystallized. However, it can be seen that the crystal structure of the silver nanoparticles does not correspond to that of the bulk solid. In general, the shapes of the various nuclei (icosahedra, decahedra, cubooctahedra and tetrahedra) are retained. No transformation such as facet truncation or preferential growth of facets occurs during the growth process. This clearly indicates that AOT surfactants forming reverse micelles do not play any role in the growth of silver nanocrystals. In other words, the water–oil interface does not induce truncation or preferential facet growth. Nanocrystals with the same shapes as the nuclei were obtained by ultra-vacuum techniques [25].

Similar behaviour is observed with copper nanocrystals [24, 25] produced at various water contents ($1.5 < w = [H_2O]/[AOT] < 15$) and a fixed reducing agent content, $R = 3$, where R is defined as $[N_2H_4]/[Cu(AOT)_2]$ (see the appendices). The TEM images of copper nanocrystals, obtained at the end of the synthesis (5 hours) vary with w (figure 3). Below $w = 10$, the average particle size increases with w but for $w > 10$ the particle size remains the same. This is explained by the increase in the number of reactants per micelle, i.e. the number of nuclei per micelle, favouring an increase in the particle size. For $w = 3$, the nanocrystals are relatively sparse on the carbon film (figure 3). Most of the entities are spherical copper particles either made of fcc clusters (figure 4A) or characterized by a more or less regular decahedral structure (figure 4D). On increasing w to 5, similar crystalline structures are produced (figure 4B, E). A further increase in w to 10 favours the increase in the number of nanocrystals characterized by a regular fcc structure attributed to cubooctahedra (figure 4C). These structures coexist with regular decahedra (figure 4D). Hence, both nanoparticle crystallinity and size increase with w (figure 4). By comparison of HRTEM and simulated images and calculated and simulated PS spectra [26] it can be concluded that monocrystal spheres and the regular decahedra result from the growth of cubooctahedra and decahedra nuclei [28], respectively. Hence, their shapes are closely related to that of the corresponding nuclei. The homogeneous growth

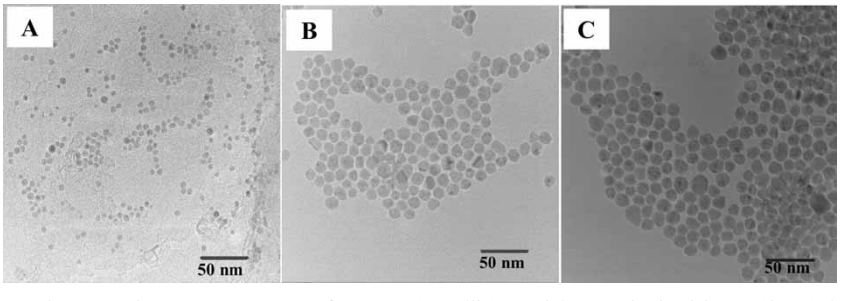

Figure 3. Electron microscopy patterns of copper (metallic) particles synthesized in $Cu(AOT)_2$/NaAOT, water, isooctane reverse micelles at various water contents. $[AOT] = 0.1$ M; $[Cu(AOT)_2] = 10^{-2}$ M. Inserts: size histograms: [A] $w = 3$; [B] $w = 5$; [C] $w = 10$.

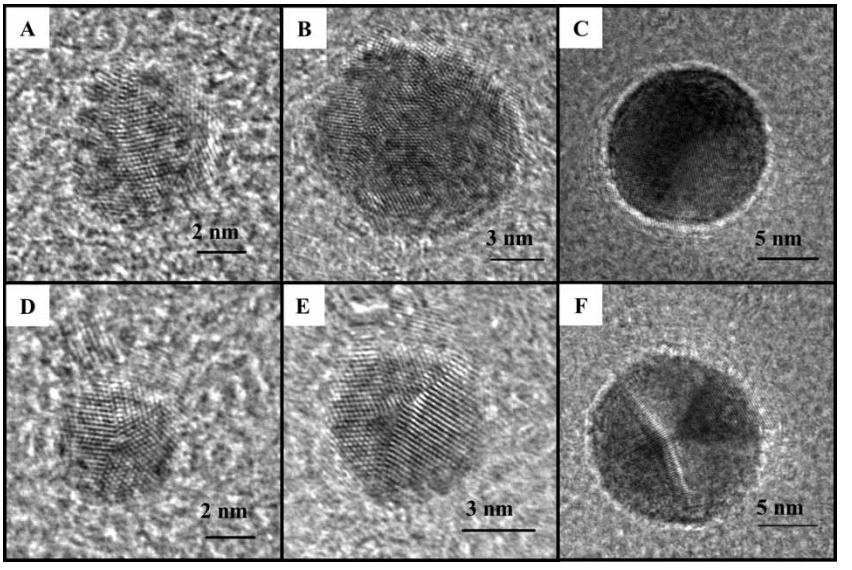

Figure 4. HRTEM images of spherical (A, B, C) and decahedral (E, F, G) copper nanocrystals synthesized in $Cu(AOT)_2$/NaAOT, water, isooctane reverse micelles at various water contents. [AOT] = 0.1 M; $[Cu(AOT)_2] = 10^{-2}$ M. [A, D] $w = 3$; [B, E,] $w = 5$; [C, F] $w = 10$.

of cubooctahedral nuclei makes possible the formation of spherical nanocrystals. Similarly, regular decahedra, formed by five deformed tetrahedral subunits twinned by their {111} planes and characterized by a five-fold symmetry, are obtained (figure 4F). The formation of such unusual structures results from the simultaneous and regular growth of the 10 enclosed {111} facets. No transformation such as facet truncation or preferential growth of facets occurs during the growth process. This confirms that AOT surfactant molecules forming reverse micelles do not play a role in such growth. It must be noted that the produced decahedra have an average size of 10–15 nm. For many years, several authors claimed that the maximal size of particles having such five-fold symmetry was around 5 nm [29]. Above this size, this structure was not considered to be stable. However large decahedra have been observed previously under ultra-vacuum [30, 31] and from colloidal solution [32]. In the first case, their stability was explained by the deformation of the tetrahedral subunits and/or the accommodation of the angle between the units.

For water contents up to 5, spheres and pentagons coexist with triangles (figure 5A–C) and elongated particles (figure 5D–F). The structure of elongated particles results from additional intermediate (110) planes in a regular decahedral nucleus and is attributed to a truncated large decahedron with five-fold symmetry as previously obtained for large nanorods grown in the presence of chloride ions [33]. In other words, their formation is induced by the truncation of the five subunit edges of the decahedral nucleus. For the triangular nanocrystals, the initial precursor nucleus must contain a unique three-fold axis, which is expressed in the final shape of the nanocrystal [34]. Only the tetrahedral nuclei can be modified simply to give a trigonal lamellar particle. The regular fcc tetrahedron is truncated on a {111} surface and then

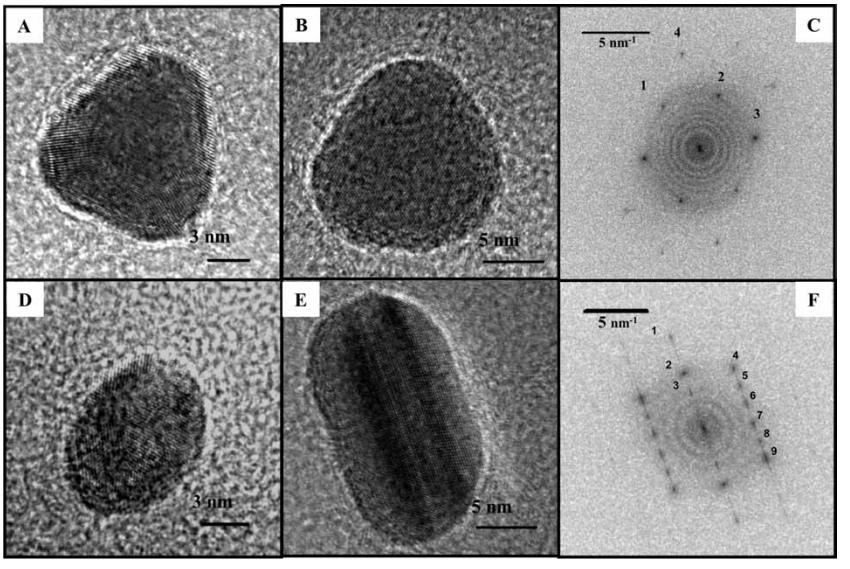

Figure 5. HRTEM images of triangles (A, B) and elongated (C, D) copper nanocrystals synthesized in $Cu(AOT)_2$/M [AQ17] NaAOT, water, isooctane reverse micelles at various water contents. [AOT] = 0.1 M; $[Cu(AOT)_2] = 10^{-2}$ M. [A, C] $w = 5$; [B,D] $w = 10$.

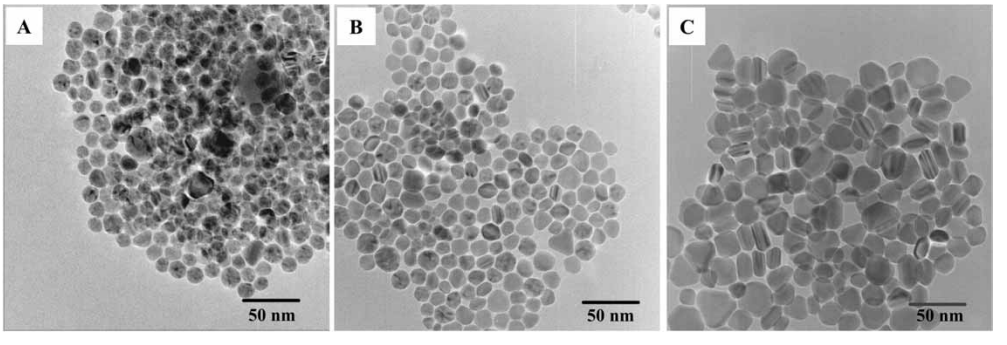

Figure 6. TEM images of copper nanocrystals obtained at various R values: (A) $R = 5$, (B) $R = 10$, (C) $R = 15$.

twinned by reflection at this surface in such a way that a suitable nucleus for the trigonal lamellar particles can be obtained. Such a bitetrahedral precursor nucleus contains the three active sites for growth to maintain the overall three-fold symmetry in the final nanocrystal [23, 26]. From these data we could expect that the supersaturation regime is a key parameter in controlling the nanocrystal shape. Let us recall the relative percentage of spheres (79%), cubes (3%), triangles (8%) and elongated particles (10%) produced when $R = 3$. To investigate the influence of the supersaturation regime on the nanocrystal shape, syntheses made at fixed water content ($w = 10$), i.e. the same droplet size and droplet concentration, and increasing the ratio R from 3

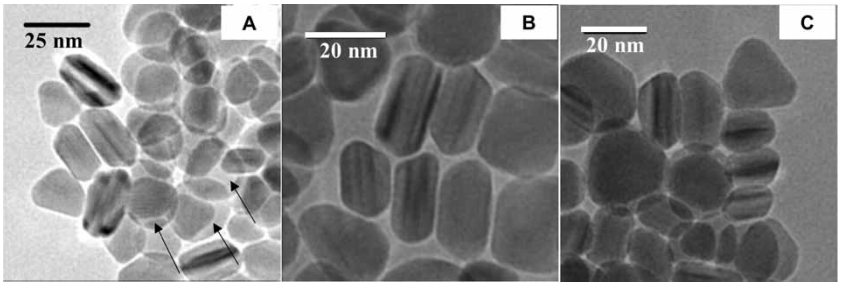

Figure 7. TEM images of copper nanocrystals on various parts of the grid.

as described above to 15 ($R = 3$, 5, 10 and 15), are carried out. Figure 6 shows the TEM images obtained for various R values [35]. At $R = 5$ the TEM images are similar to those described above for $R = 3$ with the formation of polycrystalline nanoparticles, decahedra, triangles and 'elongated' nanocrystals. On increasing R, the proportion of anisotropic shapes and sphere crystallinity markedly increases (figure 6B, C). Note that for triangular nanocrystals, the contrast is very weak, indicating the formation of very thin nanocrystals. At $R = 15$ [35], the TEM images (figure 7) show the formation of copper nanocrystals having various shapes such as spheres (20%), triangles (30%), elongated particles (30%) and cubes (9%). Note that the latter are formed by a specific growth of {111} facets of the cubooctahedral nucleus. Some nanocrystals are characterized by a very low contrast corresponding to thin copper nanocrystals and are sufficiently transparent that underlying particles are observed. The cubes and spheres are characterized by average sizes of 19 nm and 20 nm, respectively, whereas the average edge of the triangle and that of the long axis of elongated particles are 23 nm and 22 nm (with size distributions, σ, of 19% and 17%), respectively. The width and aspect ratio of elongated particles are 13 nm ($\sigma = 16\%$) and 1.8 ($\sigma = 17\%$), respectively. The HRTEM image of a triangle (figure 8A) exhibits three different lattice planes, clearly shown in the calculated power spectra (figure 8B) with three reflection pairs labelled 1, 2 and 3, and an extra reflection labelled 4. The reflections labelled 1, 2, 3 have a distance of 0.221 nm and an angle of 60° between them. This lattice parameter corresponds to the 1/3{422} reflections of the fcc structure in the [111] orientation. These reflections are forbidden for a perfect fcc crystal [23, 36–40]. The reflection labelled 4 corresponds to one of the {220} reflections of the fcc structure. The 'elongated' nanocrystals exhibit strong internal diffraction contrast which is related to defects, whose presence is confirmed by the HRTEM image (figure 8D). The corresponding power spectrum (figure 8E) shows several reflections very close to each other and attributed to defects. From a careful structural study [35], it is concluded that the triangular nanocrystals can be observed in two different orientations: [111] and [110]. Along the [111] direction, the copper nanodisk is viewed from above and triangular shapes are observed. Along the [110] direction the nanocrystal is observed from its side and in this case an elongated shape is detected. Thus, it clearly appears that the 'elongated' nanocrystals in figures 7 and 8 are copper nanodisks oriented in the [110] direction, i.e. nanocrystals oriented on the side and not 'elongated' nanocrystals.

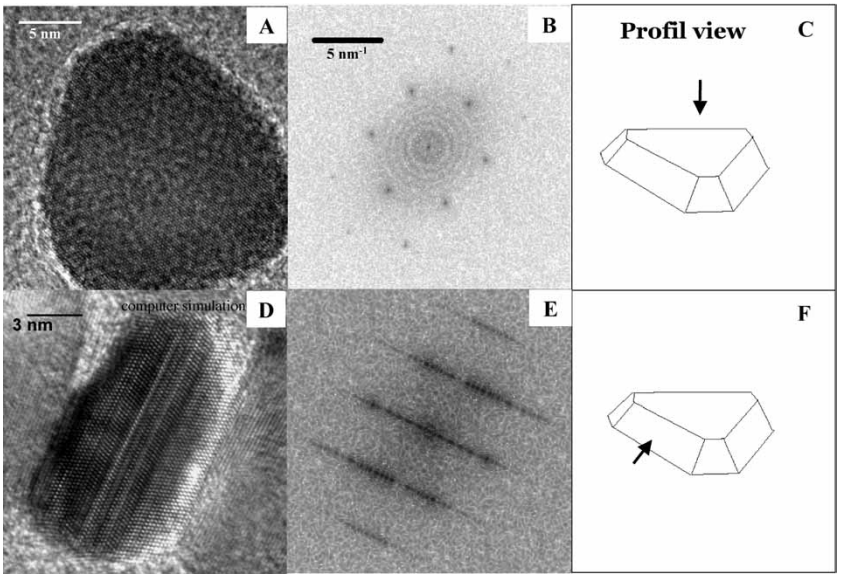

Figure 8. Triangular nanocrystals oriented in the [111] direction (A), computer simulation (B), and profile view (C). Elongated nanocrystals in the [110] orientation (D), computer simulation (E), and profile view (F). These particles were produced for $R = 15$.

Overlapped nanocrystals (figure 7C) confirm this shape while the thickness of stacked particles can be estimated (13 nm). Hence, copper nanodisks about 23 nm diameter and 13 nm thickness limited by (111) faces at the top, bottom and edges are obtained. Similar behaviour was observed previously with silver nanodisks [41] with 1/3{422} forbidden diffractions [42] for nanodisks having various shapes.

The study described above concerns silver and copper nanocrystals made in reverse micelles. In fact, similar nanodisks [41, 42] are produced by inducing a phase transition by addition of a large amount of reducing agent to reverse micelles made of a mixture of Ag(AOT) and Na(AOT) (see the appendices). The silver nanodisk size increases with the R value (figure 9). Under these experimental conditions, the surfactant moves freely in the solution during the crystal growth. At low $R = 15.6$ the average nanodisk size is 30 nm whereas it is 120 nm at $R = 39.3$. In between these R values, the nanodisk size increases progressively, as shown in figure 9. Spherical polycrystal nanoparticles are also produced. Because of the small amount of material it is impossible to give a nanodisk size distribution. For any nanodisk size, the HRTEM image of [111] orientated disks shows a perfect lattice and exhibits six-fold symmetry. The electron diffraction patterns (figure 9 inserts) exhibit six bright and sharp spots in a six-fold symmetry corresponding to {200} reflections of fcc silver single crystals orientated in the [111] direction, indicating that the flat surface of the disks is parallel to the (111) habit plane. The diffraction pattern also shows 1/3{422} reflections which are, as already mentioned, formally forbidden for a perfect fcc structure. The same spots are observed for any nanodisk size (figure 9 inserts). However, it can be noticed that the intensity differs from one sample to another. The 1/3{422} forbidden reflection on the [111] pattern has been observed previously in plate-like Au and silver

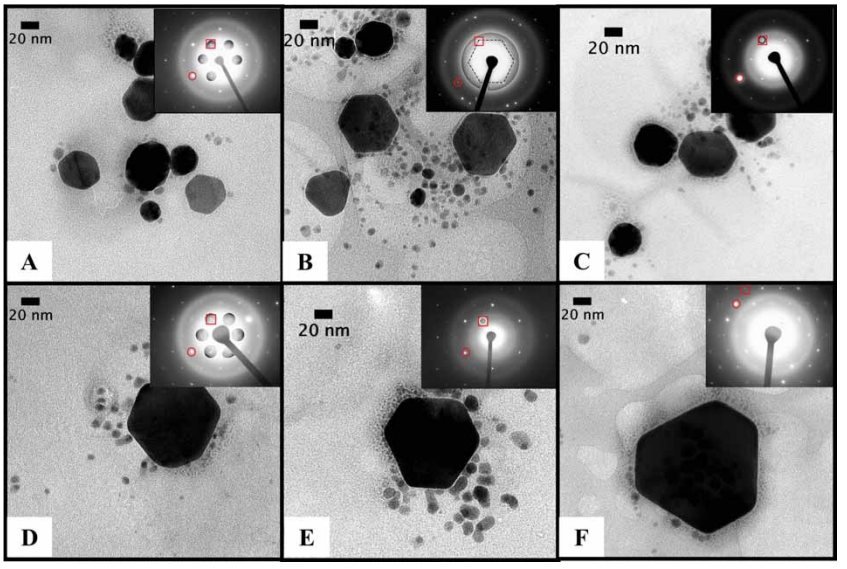

Figure 9. TEM images of silver nanodisks produced at various R values. (A) $R = 15.6$, $S = 30$ nm; (B) $R = 21$, $S = 40$ nm; (C) $R = 23.7$, $S = 50$; (D) $R = 26.3$, $S = 60$ nm; (E) $R = 32.7$, $S = 80$ nm; (F) $R = 39$, $S = 120$ nm. Inserts: diffraction patterns of isolated nanodisks. All patterns show the 1.3{422} forbidden reflections (see the squares). This figure is available in colour online.

nanocrystals [23, 39, 43–46]. A careful study [42] shows that the unique (111) stacking fault, parallel to the (111) planes, explains the 1/3{422} forbidden reflections in 111 selected area electron diffraction patterns.

4. Discussion

The reduction by hydrazine of functionalized surfactant forming reverse micelles produces silver and copper nanoparticles with good crystallinity when the number of reactants per micelle is large (up to 2) and the synthesis takes place in the saturation regime ($R = [N_2H_4]/[AOT] > 2$). At rather low R values (R around 2 or 3), the structures of the produced nanoparticles are similar to those of nuclei. Hence silver and copper nanocrystals having icosahedral, decahedral and cubooctahedral structures were both formed. This clearly shows the homogeneous growth of the four nuclei (icosahedra, decahedra, cubooctahedra and tetrahedra) inside the micelles. These data indicate positively that, by reduction with hydrazine of copper and silver ions, homogeneous growth of nuclei inside the reverse micelles takes place. The average silver nanocrystal size is around 5 nm. This corresponds to the particle size limit proposed by several authors for making five-fold symmetry particles such as decahedra [29]. With copper nanocrystals, the average size of decahedra is quite large (around 20 nm) as observed previously in colloidal solution [32]. This could be attributed to the fact that AOT surfactant molecules forming reverse micelles favour the stability of nanocrystals by selective adsorption on the {111} facets. However, large decahedra have also been

observed previously under ultra-vacuum [30, 31] suggesting that AOT reverse micelles play a minor role in the nanocrystal growth. Large cubooctahedral nanocrystals are also produced. Hence, the apparently spherically shaped nanocrystals are directly related to the crystallographic phase of the nuclei. From these data it is concluded, conversely to what is observed with other synthesis methods [47–52], that the role of the surfactant molecules is minor when they are self-assembled in oil-rich colloidal solutions [26, 27, 32, 35, 53–57]. This is probably due to the fact that in such water-in-oil solutions the surfactant molecules stay at the oil–water interface and are not free in the bulk phase. This markedly differs from the water-rich colloids where some of the surfactant molecules are self-assembled whereas others remains free in the water phase. It is found that in oil-rich colloidal solutions, the addition of a very low percentage of salt induces a drastic change in the shape [32, 33, 53]. This means that residual impurities coming from the production of the functional surfactant could also play a role in the shape control. This could explain slight discrepancies in the shape control between the data obtained many years ago [54, 55] and those published recently [26, 27, 35].

Figure 5 shows the formation of elongated particles and triangles for $R = 3$ and $w = 10$. The first nanocrystals originate from decahedra with additional intermediate (110) planes in the regular decahedral nucleus. This confirms data obtained previously with copper nanorods produced in the presence of a small amount of chloride salt [33] and in a given part of the phase diagram [54, 55]. In the triangular nanocrystals, the nucleus is made up of tetrahedral nuclei containing the three-fold axis expressed in the final shape of the nanocrystal [34]. To explain such truncations and/or additional planes we have to assume that the amount of hydrazine is a key parameter in the control of these shapes. In fact, the influence of the AOT surfactant cannot be taken into account because quite a large number of nanocrystals keep the same structure as the initial nuclei. This claim is confirmed from data obtained on increasing the R values. Let us consider the relative percentages of various shapes obtained at low ($R = 3$) and large ($R = 15$) R values. On increasing R, the percentage of spheres (including pentagonal and regular spherical shapes) drops from 79% to 30%, that of the cubes increases from 3% to 9%, that of the elongated particles increases from 10% to 30% and that of triangles increases from 8% to 30%. Note that isocoahedral particles are not stable enough at their sizes compared with decahedra. From the above, spheres are produced mainly by decahedra and cubooctahedra. In addition, more cubes are formed by a specific growth of {111} facets of the cuboctahedral nucleus. For $R = 3$ the elongated nanocrystals are mainly truncated decahedra with no detected nanodisks. From this it is concluded that 92% of the nuclei are decahedra and cubooctahedra. The remaining nanocrystals (8%) are triangles characterized by a three-fold symmetry and produced from tetrahedral nuclei. When $R = 15$ most of the elongated particles are in fact nanodisks sitting on 110 facets. Very few truncated decahedron nanocrystals are observed. To a first approximation, we estimate that less than 10% of the elongated particles have a truncated decahedron structure and consequently more than 50% are copper nanodisks (triangles) sitting on either the [111] or [110] directions, i.e. more than 65% (two subunits for a nanodisk) of tetrahedral nuclei are produced. Hence on increasing R from 3 to 15, the number of tetrahedral nuclei increases from 17% to more than 65%. Thus hydrazine seems to favour the formation of tetrahedral nuclei. This

is rather surprising and needs to be explained. For silver nanodisks it is impossible to make a qualitative estimation of the increase in the amount of the produced nanodisks. Nevertheless similar behaviour is observed. With copper the nanodisk edges are smooth, whereas with silver the truncations markedly differ from one particle to another making it difficult to have a good size selection [58]. The major differences in the syntheses of copper and silver nanocrystals are related to the fact that copper disks are made in reverse micelles whereas the silver disks are produced by inducing a phase transition during the hydrazine addition. This results in a drastic change in the self-organization of surfactant molecules. The well-defined water-in-oil interface with all the self-assembled surfactant molecules disappears and AOT molecules move freely in the solution. This could favour selective adsorption of the surfactant on given facets with marked changes in the truncations because of the very similar values of the surface energy of the facets. In both cases (copper and silver nanocrystals) and for any nanodisk size, the nanodisks orientated along the [111] direction show a perfect lattice with six-fold symmetry corresponding to {200} reflections of fcc single crystals with a flat surface parallel to the (111) habit plane. Similarly, those resembling elongated particles are nanodisks oriented along the [110] plane. In both cases (copper and silver), as observed by others for plate-like particles [23, 39, 43–46], forbidden diffractions for a perfect fcc structure (1/3{422} reflections) are observed. The unique (111) stacking fault parallel to the (111) planes could be the key factor in the formation and growth of nanodisk morphology. In fact, the shape of a plate-like nanocrystal is determined by the crystal growth occurring along the [111] direction, i.e. in the twin planes. Then, it is reasonable to assume that a stacking fault promotes growth parallel to the (111) planes leading to the plate-like shape. From the fcc tetrahedral precursor, a twin plane is formed when two regular nuclei truncated on a {111} surface stick together [23]. This leads to a bitetrahedral nucleus having the required three-fold symmetry for the triangular nanodisks. On the other hand, its re-entrant intersections of {111} faces at a twin plane are three active sites for accelerated growth maintaining the overall three-fold symmetry in the final nanocrystal. The truncations are attributed to the capping of hydrazine on the edges favouring the formation of multiple twinned particles by decreasing the stacking fault energy of fcc copper structures, leading to nanodisk morphologies. In the case of silver nanodisks, adsorption of the surfactant could explain the various truncations observed with silver nanodisks and confirmed via their optical properties [58] whereas with copper nanodisks the optical properties confirm mainly the same nanodisk snip [59].

5. Conclusions

In this paper we have demonstrated that reverse micelles make it possible to produce silver and copper nanocrystals having the same shapes as their nuclei. This clearly indicates that there can be homogeneous growth of nanocrystals with a water–oil interface. Furthermore, on increasing the amount of reducing agent such as hydrazine, the number of copper tetrahedral nuclei increases, favouring formation of nanodisks with a rather low size and shape distribution. Silver nanodisks are also produced by inducing a phase transition. The structure of both nanodisks are identical with the

formation of pure fcc monocrystals and a forbidden diffraction for an fcc structure (1/3{422} reflections). This unique (111) stacking fault parallel to the (111) planes could be the key factor in the formation and growth of nanodisk morphology. In the case of silver, the nanodisks are characterized by various truncations and also seems to be thicker than those produced with copper. This is probably due to the fact that the free surfactant molecules produced during the phase transition specifically adsorb on given facets. These data diverge from those usually published claiming the surfactant plays a key role in the nanocrystal growth. That could be the case for either 'free' surfactant molecules in solution or normal micellar solution where free molecules coexist with the aggregates. The discrepancies observed by using reverse micelles are probably due to impurities in the surfactant production. For example, we know that addition of a homeopathic quantity of salts can drastically break the crystal growth keeping the micellar structure intact.

Acknowledgments

This paper could not have been written without taking into account the data obtained over the last few years by colleagues in my laboratory. I am very grateful to Drs A. Courty, D. Ingert, V. Germain, C. Salzemann and especially to Dr I. Lisiecki who made several constructive comments. Thanks are also due to Dr. Ngo who took care of the final version of the paper and to Professor J. Urban from the Max Plank Institute in Berlin. Finally, I wish to thank to the EU for funding (GSOMEN project NMP4-CT-2004-001594).

Appendix A. Syntheses in reverse micelles

A.1. *Silver nanocrystals* [5, 60, 24]

The 5 nm silver colloidal particles are produced by mixing two micellar solutions. The first one contains 3 ml of 0.1 M Ag(AOT), & 2 ml of 0.1 M Na(AOT). The second one consists of 5 ml of 0.1 M Na(AOT) containing 25 μl of hydrazine. Assuming the density of hydrazine is that of water, the overall water content, defined as $w = [H_2O]/[AOT]$, is $w = 2$. The ratio R, defined as $R = [N_2H_4]/[Ag(AOT)]$, is 2.4. Dodecanethiol ($2\,\mu l/cm^3$) is then added to the solution and a selective reaction with silver atoms at the interface of the particles takes place. Ethanol is next added to this solution, inducing flocculation of the dodecanethiol-coated silver particles, and the precipitate is then dispersed in hexane. To reduce the size distribution, a size selected precipitation process is used: pyridine is progressively added to hexane solution containing the silver-coated particles. Silver nanoparticles (5 nm diameter) are thus obtained with a rather low size distribution (around 13%). By deposition of two drops of a low-concentration solution on a cleaved carbon substrate, a monolayer made of nanoparticles with a spontaneous hexagonal organization is produced.

A.2. *Copper nanocrystals* [56, 26, 27, 35]

A mixture of surfactants, 10^{-2} M $Cu(AOT)_2$ and 10^{-1} M NaAOT where AOT is bis (2-ethylhexyl)sulfosuccinate, is solubilized in isooctane and forms spherical reverse micelles. Copper nanocrystals are obtained by reduction of $Cu(AOT)_2$ by hydrazine (N_2H_4). The ratio R, defined as $R = [N_2H_4]/[Cu(AOT)_2]$, varies from 3 to 15, corresponding to changes in the hydrazine concentration from 3×10^{-2} M to 0.15 M. In order to ensure that the data are as consistent as possible, we assumed that a molecule of water has the same volume as that of a molecule of hydrazine and both contribute similarly to the polar volume fraction. The overall water content varies from 1.5 to 15. After hydrazine addition, the solution immediately turns dark, indicating the reduction of Cu^{2+} to Cu^0. At the end of the chemical reaction (5 h), a few drops of the colloidal solution are deposited on an amorphous carbon film supported by a copper grid and allowed to evaporate. In order to prevent oxidation the reaction takes place in an inert atmosphere.

Appendix B. Synthesis in the presence of 'free' surfactant [41, 61].

Silver nanodisks are obtained by mixing two solutions:

(i) The first solution contains reverse micelles made of 60% 0.1 M Ag(AOT) (silver di(2-ethyl-hexyl)sulfosuccinate) and 40% 0.1 M Na(AOT) solubilized in isooctane. The water content, $w = [H_2O]/[AOT]$, is kept at 2.

(ii) The second solution is 0.1 M Na(AOT) in isooctane, with water replaced by the reducing agent, hydrazine (N_2H_4) in the ratio $R = [N_2H_4]/[Ag(AOT)]$. The overall hydrazine concentration varies from 0.5 M to 1.66 M and its content, defined as $R = [N_2H_4]/[Ag(AOT)]$, varies from 15.6 to 39.3. The solution, stirred for 20 min, becomes opalescent because a phase transition takes place; reverse micelles are no longer formed.

The two solutions are mixed together and a dark colour quickly appears. The solution is then diluted 100 times in 0.1 M Na(AOT) solution and subjected to ultrasound for 10 min. The colour of the solution depends on the initial synthesis conditions, from red for the lowest reducing agent ratio, to green and grey for the highest. The solution remains stable for several months.

References

[1] J. R. Heath. Accounts of Chemical Research, Special issue on Nanoscale Materials. Guest editor **32,** 388 (1999).
[2] D. Vollath, D. V. Szabo, R. D. Taylor, and J. O. Willis. Synthesis and magnetic properties of nanostructured maghemite. J. Mat. Res. **12,** 2175 (1997).
[3] A. Perez. Nanostructured materials from clusters: synthesis and properties. Materials Transactions **42,** 1460 (2001).
[4] C. B. Murray, D. J. Norris, and M. G. Bawendi. Synthesis and characterization of nearly monodisperse CdE (E = sulfur, selenium, tellurium) semiconductor nanocrystallites. J. Am. Chem. Soc. **115,** 8706 (1993).
[5] M. P. Pileni. Reverse micelles: a microreactor. J. Phys. chem. **97,** 6961 (1993).
[6] M. P. Pileni. Nanosized particles made in colloidal assemblies. Langmuir **13,** 3266 (1997).

[7] M. P. Pileni. Mesostructured fluids in oil rich regions: structural and templating approaches. Langmuir **17,** 7476 (2001).
[8] V. M. Cepak and C. R. Martin. Preparation and stability of template synthesized metal nanorod sols in organic solvents. J. Phys. Chem. **102,** 9985 (1998).
[9] M. E. Toimil Molares, V. Buschmann, D. Dobrev, R. Neumann, R. Scholz, I. U. Schuchert, and J. Vetter. Single crystalline copper nanowires produced by electrochemical deposition in polymeric ion track membrane. Adv. Mater. **13,** 62 (2001).
[10] H. Namatsu, K. Kurihara, M. Nagase, and T. Makino. Fabrication of 2-nm wide silicon quantum wires through a combination of a partially shifted resist pattern and orientation dependent etching. Appl. Phys. Lett. **70,** 619 (1997).
[11] J. Wang, D. A. Thomson, B. J. Robinson, and J. G. Simmons. Molecular beam epitaxial growth of InGaAs/InGaAsP quantum wires on V-grooved InP substrates with (111) sidewalls. J. Cryst. Growth. **175,** 793 (1997).
[12] S. A. Nepijko, D. N. Ievlev, W. Schulze, J. Urban, and G. Ertl. Growth of rodlike silver nanoparticles by vapor deposition of small clusters. Chem. Phys. Chem. **1,** 140 (2000).
[13] Y. Y. Yu, S. S. Chang, C. L. Lee, and C. R. Chris Wang. Gold nanorods: electrochemical synthesis and optical properties. J. Phys. Chem. B. **101,** 6661 (1997).
[14] L. Huang, H. Wang, Z. Wang, A. Mitra, K. N. Bozhilov, and Y. Yan. Nanowires arrays electrodeposited from liquid crystalline phases. Adv. Mater. **14,** 61 (2002).
[15] Z. L. Wang, R. P. Gao, B. Nikoobakht, and M. A. El Sayed. Surface reconstruction of unstable [110] surface in gold nanorods. J. Phys. Chem. B. **104,** 5417 (2000).
[16] I. Lisiecki. Size, shape and structural control of metallic nanocrystals. J. Phys. Chem. B. **109,** 12231 (2005).
[17] R. Boistelle. *Industrial Crystallization*, edited by J. W. Mullin (Pub. Plenum Press, New York, 1976) pp. 203–214.
[18] *Reverse Micelles*, edited by M. P. Pileni (published Elsevier, 1989).
[19] L. Motte, I. Lisiecki, and M. P. Pileni. Role of water molecules in the growth of nanosizes particles in reverse micelles. edited by J. Dore and M. C. Bellisan (Hydrogen Bond Networks NATO. Publisher) 447 (1994).
[20] M. P. Pileni, B. Hickel, C. Ferradini, and J. Pucheault. Hydrated electron in reverse micelles. Chem. Phys. Lett. **92,** 308 (1982).
[21] C. Petit and M. P. Pileni. Cadmium sulfite synthetized in "situ" in reverse micelles. J. Phys. Chem. **92,** 2282 (1988).
[22] C. Petit, P. Lixon, and M. P. Pileni. Synthesis in situ of cadmium sulfate semiconductor: -2- effect of functionalized surfactant. J. Phys. Chem. **94,** 1598 (1990).
[23] A. I. Kirkland, D. A. Jefferson, D. G. Duff, P. P. Edwards, I. Gameson, B. F. G. Johnson, and D. J. Smith. Structural studies of trigonal lamellar particles of gold and silver. Proc. R. Soc. Lond. A. **440,** 589 (1993).
[24] A. Courty, I. Lisiecki, and M. P. Pileni. Vibration of self organized silver nanocrystals. J. Chem. Phys. **116,** 8074 (2002).
[25] J. Urban, H. Sack-Kongehl, and K. Weiss. Computer simulations of HREM images of metal clusters. Zeitchrift Für Physik D **28,** 247 (1993).
[26] C. Salzemann, I. Lisiecki, J. Urban, and M. P. Pileni. Anisotropic growth of copper nanocrystals synthesized in a supersaturated medium: structural study. Langmuir **20,** 11772 (2004).
[27] C. Salzemann, I. Lisiecki, A. Brioude, J. Urban, and M. P. Pileni. Collections of copper nanocrystals characterized by different sizes and shapes: optical response of these particles. J. Phys. Chem. B. **108,** 13242 (2004).
[28] J. Urban. Crystallography of clusters. Cryst. Res. Technol. **33,** 7 (1998).
[29] D. Reinhard, B. D. Hall, P. Berthoud, S. Valkealahti, and R. Monot. Unsupported nanometer sized copper clusters studied by electron diffraction and molecular dynamics. Phys. Rev. B. **58,** 4917 (1998).
[30] J. L. Gardea-Torresday, K. L. Tiemann, G. Gamez, K. Dokken, S. Tehuacanero, and M. J. Yacaman. Gold nanoparticles obtained by bio-precipitation from gold(III) solutions. J. Nanoparticle Res. **1,** 397 (1999).
[31] S. Ijima. Fine particles of silicon. I. Crystal growth of spherical particles of Si. Jpn. J. Appl. Phys. Part **26,** 357(1) (1987).
[32] A. Filankembo, S. Giorgio, I. Lisiecki, and M. P. Pileni. Is the anion the major parameter in the shape control of nanocrystals?. J. Phys. Chem. B. **107,** 7492 (2003).
[33] I. Lisiecki, A. Filankembo, H. Sack-Kongehl, K. Weiss, M. P. Pileni, and J. Urban. Structural investigations of copper nano-rods by HRTEM. Phys. Rev. B. **61,** 4968 (2000).
[34] T. S. Ahmadi, Z. L. Wang, A. Henglein, and M. A. El-sayed. ≪Cubic≫ colloidal platinum nanoparticles. Chem. Mater. **8,** 1161 (1996).

[35] C. Salzemann, I. Lisiecki, J. Urban, and M. P. Pileni. Characterization and growth process of copper nanodisks. Adv. Funct. Materials **15,** 1277 (2005).
[36] T. Hayashi, T. Ohno, S. Yatsuya, and R. Uyeda. Formation of ultrafine metal particles by gas-evaporation technique. IV. Crystal habits of iron and Fcc metals, Al, Co, Ni, Cu, Pd, Ag, In, Au and Pb. Japan J. Appl. Phys. **16,** 705 (1977).
[37] G. Nihoul, K. Abdelmoula, and J. J. Métois. Formation of ultrafine metal particles by gas-evaporation technique. IV. Crystal habits of iron and Fcc metals, Al, Co, Ni, Cu, Pd, Ag, In, Au and Pb. Ultramicroscopy **12,** 353 (1987).
[38] R. H. Morriss, W. R. Bottoms, and R. G. Peacock. Growth and defect structure of lamellar gold microcrystal. J. Appl. Phys. **39,** 3016 (1968).
[39] J. C. Heyraud and J. J. Métois. Anomalous 1/3 422 diffraction spots from {111} flat gold crystallites: (111) surface reconstruction and moiré fringes between the surface and the bulk. Surf. Sci. **100,** 519 (1980).
[40] V. Castano, A. Gomez, and M. Yacaman. Microdiffraction and surface structure of small gold particles. Surf. Sci. **146,** L587 (1984).
[41] M. Maillard, S. Giorgio, and M. P. Pileni. Silver Nanodisks. Adv. Mat. **14,** 15 (2002).
[42] V. Germain, J. Li, D. Ingert, Z. L. Wang, and M. P. Pileni. Stacking falts in formation of silver nanodisks. J. Phys. Chem. B. **107,** 34 (2003).
[43] R. Jin, Y. W. Cao, C. A. Mirkin, K. L. Kelly, G. C. Schartz, and J. C. Zheng. Photoinduced conversion of silver nanospheres to nanoprisms. Science **294,** 1901 (2001).
[44] D. Cherns. Direct resolution of surface atomic steps by transmission electron microscopy. Philos. Mag. **30,** 549 (1974).
[45] A. I. Kirkland, D. A. Jefferson, D. G. Duff, and P. P. Edwards. High resolution studies of trigonal lamellar particles of gold and silver. Inst. Phys. Conf. Ser. **98,** 37 (1989).
[46] N. Tanaka and J. L. Cowley. Studies of planar defects in silver plate-like crystals by CBED and HRTEM techniques. Mat. Res. Soc. Symp. Proc. **41,** 155 (1985).
[47] S. Wang and S. Yang. Preparation, and characterization of oriented PbS crystalline nanorods in polymer films. Langmuir **16,** 389 (2000).
[48] L. Manna, E. C. Scher, and A. P. Alivisatos. Synthesis of soluble and processable rod-, arrow-, teardrop-, and tetrapod-shaped CdSe nanocrystals. J. Am. Chem. Soc. **122,** 12700 (2000).
[49] V. F. Puntes, K. M. Kristhnan, and A. P. Alivisatos. Colloidal nanocrystal shape and size control: the case of cobalt. Science. **291,** 2115 (2001).
[50] S. J. Park, S. Kim, S. Lee, Z. G. Khim, K. Car, and T. Hyeon. Synthesis and magnetic studies of uniform iron nanorods and nanospheres. J. Am. Chem. Soc. **122,** 8581 (2000).
[51] N. R. Jana, L. Gearheart, and C. J. Murphy. Wet chemical synthesis of silver nanorods and nanowires of controllable aspect ratio. Chem. Comm. **7,** 617 (2001).
[52] N. R. Jana, L. Gearheart, and C. J. Murphy. Wet chemical synthesis of high aspect ratio cylindrical gold nanorods. J. Phys. Chem. B. **105,** 4065 (2001).
[53] J. Tanori and M. P. Pileni. Change in the shape of copper nanoparticles in ordered phases. Adv. Mater. **7,** 862 (1995).
[54] J. Tanori and M. P. Pileni. Control of the shapes of copper metallic particles by using colloidal system as template. Langmuir **13,** 639 (1997).
[55] M. P. Pileni, T. Gulik-Krzywicki, J. Tanori, A. Filankembo, and J. C. Dedieu. Template design of microreactors with colloidal assemblies: control the growth of copper metal rods. Langmuir **14,** 7359 (1998).
[56] I. Lisiecki and M. P. Pileni. Synthesis of copper metallic clusters by using reverse micelles as microreactors. J. Am. Chem. Soc. **115,** 3887 (1993).
[57] I. Lisiecki and M. P Pileni. Control of the shape and the size of copper metallic particles. J. Phys. Chem. **100,** 4160 (1996).
[58] V. Germain, A. Brioude, D. Ingert, and M. P. Pileni. Silver nanodisks: size selection via centrifugation process and optical properties. J. Chem. Phys. **122,** 124707 (2005).
[59] C. Salzeman, A. Brioude, and M. P. Pileni. Optical properties of copper nanocrystals differing by their shapes (to be sent for publication).
[60] A. Taleb, C. Petit, and M. P. Pileni. Synthesis of highly monodisperse silver nanoparticles from AOT reverse micelles: a way to 2D and 3D self-organization. Chem. Mater. **9,** 950 (1997).
[61] M. Maillard, S. Giorgio, and M. P. Pileni. Tuning the size of silver nanodisks with similar aspect ratio: synthesis and optical properties. J. Phys. Chem. B. **107,** 2466 (2003).